CORRECTION NOTICE

Nat. Med. **20,** 778–784 **(2014)**

On-demand intracellular amplification of chemoradiation with cancer-specific plasmonic nanobubbles

Ekaterina Y Lukianova-Hleb, Xiaoyang Ren, Rupa R Sawant, Xiangwei Wu, Vladimir P Torchilin & Dmitri O Lapotko

In the version of this supplementary file originally posted online, the figure legend for Supplementary Fig. 5d was incorrect. It should have read as follows:
"Scans of GNP-treated animal: PNB signal amplitudes for primary tumor (solid green), surgical margins after tumor resection (solid red) and primary tumor in intact animal that was not treated with GNPs (solid black), standard photoacoustic small animal imaging system (Vevo LAZR, Visual Sonics) signals for the same animals with untreated (black dashed line) and GNP-treated primary tumors (red dashed line)."
The error has been corrected in this file as of 17 November 2014.

SUPPLEMENTARY INFORMATION

On-demand intracellular amplification of chemoradiation with cancer-specific plasmonic nanobubbles

Ekaterina Y. Lukianova-Hleb, Rupa R. Sawant, Xiaoyang Ren, Xiangwei Wu,
Vladimir P.Torchilin, Dmitri O. Lapotko

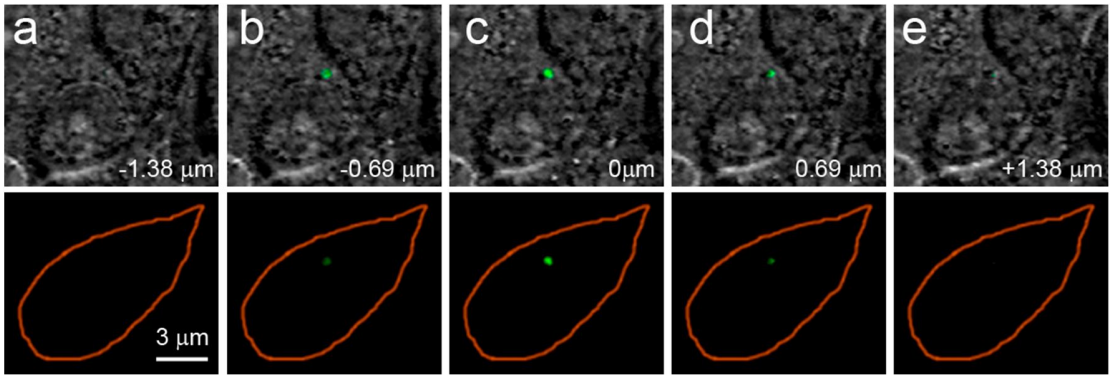

Supplementary Figure 1. The confocal images of HN31 cells treated with GNP-C225 conjugates and Calcein-Green loaded liposomes conjugated with 2C5 antibody and exposed by a single laser pulse (70 ps, 532 nm, 40 mJ cm^{-2}). Top: merged bright field and fluorescence images of the cells at different distances. Bottom: the fluorescence images of the same cells. The images were selected from the Z-stack obtained by using a LSM710 laser confocal microscope. Calcein Green excitation/emission/ bandpass wavelength: 488/530/25 nm.

Comments to Supplementary Figure 1. The cancer HN31 cells were incubated with GNP-C225 conjugates ($2.4x10^{10}$ GNPs ml^{-1}) and Calcein Green – loaded liposomes conjugated with 2C5 antibody[1] for 24 hours at 37°C. The unbound GNPs and liposomes were washed off prior to laser treatment (70 ps, 532 nm, 40 mJ cm^{-2}). Thus the cells were exposed only to the internalized GNP and liposomes

during the follow-up generation of plasmonic nanobubbles (PNBs). A LSM 710 laser confocal microscope was used in fluorescence and scattering (under excitation with a 633 nm continuous laser) modes for detection and analysis of GNPs and liposome-specific green fluorescence in individual living cells before and from 10 minutes to 5 hours after the exposure to a laser pulse (Fig. 2a). The pixel image amplitudes were measured locally in each individual cell for at least 150-180 cells per sample (three samples were studied) and were then analyzed as the population-averaged metrics of GNP cluster formation (Supplementary Fig. 4) and dye release (green fluorescence) (Fig. 2e).

Three-dimensional confocal imaging of living cells was performed to evaluate the location and co-localization of liposome-associated dye release and GNP clusters in cells immediately after the exposure to the laser pulse. To do this, the LSM 710 laser confocal microscope was used in a Z-stack mode with 0.69 μm layer thickness (Supplementary Fig. 1). The obtained images confirm the intracellular dye release via the mechanical disruption of the dye-loaded liposomes and cellular endosomes during PNB expansion and the ejection of the dye into the cytoplasm of cells where PNBs were generated.

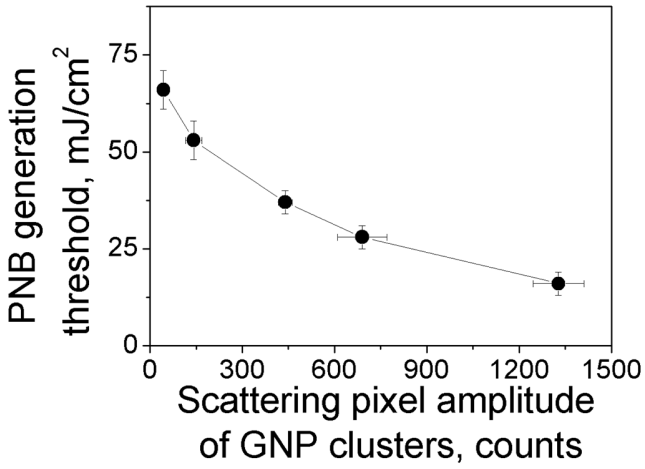

Supplementary Figure 2. PNB generation threshold fluence of the excitation laser pulse as a function of GNP cluster size (measured through scattering pixel amplitude of GNP cluster image in individual cells) [134].

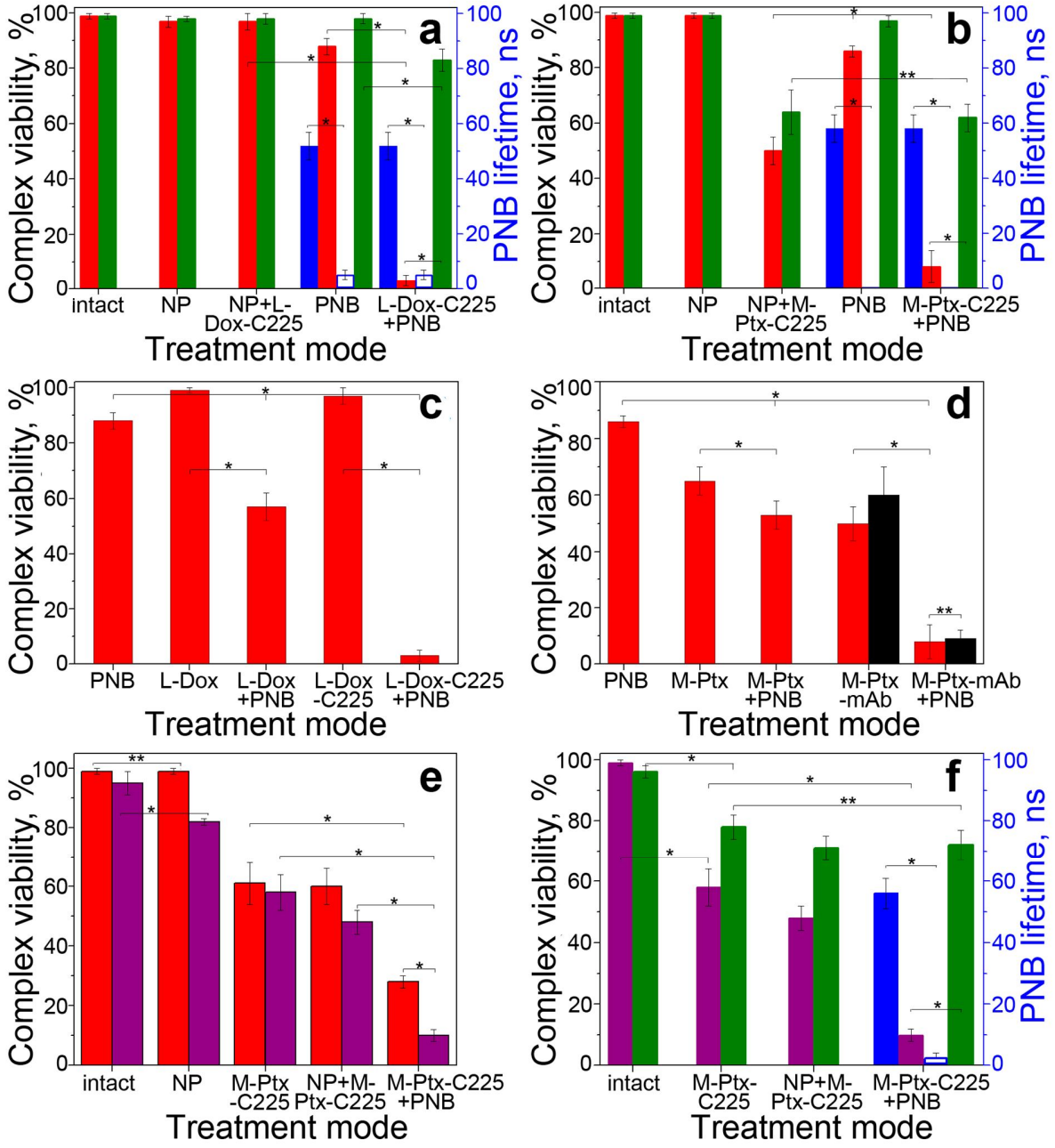

Supplementary Figure 3. The complex viability of cells: (**a**): treatment with liposomal Doxil, (**b**): treatment with micellar paclitaxel. Cancer (HN31, *solid red*) and normal (NOM9, *solid green*) cells measured 72 h after applying specific treatments. *Blue* bars show the PNB lifetime in cancer (*blue solid*) and normal (*blue hollow*) cells. The treatment modes: I: intact cells; GNP: cells treated by gold 60 nm spheres conjugated with C225; GNP+Dox: cells treated with GNP and soluble encapsulated drug doxorubicin (Doxil), 5 μg ml^{-1}, conjugated with C225; PNB: single laser pulse applied to GNP-C225-treated cells; Dox+PNB: single laser pulse was applied to GNP-C225- and Doxil-C225-treated cells. GNP+Ptx: GNP and encapsulated poorly soluble drug paclitaxel (Ptx), 0.065 μg ml^{-1}, conjugated

with C225; Ptx+PNB: single laser pulse was applied to GNP-C225- and Ptx-C225-treated cells. Laser treatment was a single pulse, 70 ps, 532 nm, 40 mJ cm^{-2}. * $P < 0.05$, ** $P > 0.05$. (**c**): PNB: single laser pulse applied to GNP-C225-treated cells; Dox: cells treated with plain doxorubicin-loaded liposomes; Dox+PNB: single laser pulse applied to GNP-C225- and plain doxorubicin-loaded liposomes-treated cells; Dox-C225: cells treated with conjugated doxorubicin-loaded liposomes; Dox-C225+PNB: single laser pulse applied to GNP-C225- and Dox-C225-treated cells. (**d**) Ptx: plain paclitaxel-loaded micelles-treated cells; Ptx+PNB: single laser pulse applied to GNP-C225- and plain paclitaxel-loaded micelles-treated cells; Ptx-mAb: cells treated with conjugated paclitaxel-loaded micelles; Ptx-mAb+PNB: single laser pulse applied to GNP-C225- and conjugated (C225) paclitaxel-loaded micelles-treated cells. The effect of dual targeting with Ptx-2C5 and GNP-C225 (*black*, the above conjugates are shown as Ptx-mAb) (* $P < 0.05$, ** $P > 0.05$). (**e**) Effect of a single X-ray dose (10 Gy) applied within 30 min after treatment to cancer cells (*red* – without X-rays, drug dose reduced to 0.05 μg ml^{-1}; *purple* – with X-rays). (**f**) The effect of a single X-ray dose (10 Gy) on cancer (*purple*) and normal (*green*) cells pre-treated as in (Supplementary Fig. 3b) under the reduced concentration of Ptx (0.05 μg ml^{-1}). *Blue* bars show the PNB lifetime in cancer (*solid*) and normal (*hollow*) cells. Laser treatment was a single pulse, 70 ps, 532 nm, 40 mJ cm^{-2}. * $P <0.05$, ** $P > 0.05$

Comments to Supplementary Figure 3a,b. We used EGFR-positive HN31 (cancer) cells and EGFR-negative NOM9 (normal) cells. Drug carriers and GNP-C225 conjugates ($2.4x10^{10}$ GNPs ml^{-1}) were separately administered to cells (for 24 hours with Doxil-C225 (Dox, 5 μg ml^{-1}) and for 4 hours with micellar Paclitaxel-C225 (Ptx, 0.065 μg ml^{-1})) and were then washed off prior to laser treatment (70 ps, 780 nm, of 45 mJ cm^{-2}). After incubation, GNPs and drug carriers were washed off. Thus the cells were exposed only to the internalized drug during the follow-up generation of PNBs. PNB lifetime was obtained for individual cells. The short-term viability was evaluated 72 hours after the treatment of samples as a complex viability parameter *RRV* that included the viability level V_l (measured in % with Trypan Blue exclusion test) and the cell concentration *C*: $RRV=C/C_0*V_l$, * 100% , where C_0 is the cell concentration in the intact sample.

The effect of PNBs alone (without any drug) after a single laser pulse was found to be almost non-invasive: PNBs with 50-60 ns lifetimes that were observed mainly in target cells (shown in blue in

Supplementary Fig. 3a,b) did not significantly reduce their viability (Supplementary Fig. 3a,b). However, in target cells treated with nanocarriers and PNBs, there was a tremendous reduction in their viability: it dropped from 88% (PNBs alone) to 3% in the Dox treated target cells (Supplementary Fig. 3a) and from 86% (PNBs alone) to 8% in Ptx treated non-target cells (Supplementary Fig. 3b). In contrast to target cells, the identically treated non-target cells demonstrated a much better survival rate: 83% for Dox treated cells and 62% for Ptx treated cells (Supplementary Fig. 3a,b). In these experiments the PNB lifetime correlated well to the decrease in cell viability in cells treated both with therapeutic nanocarriers and PNBs (Supplementary Fig. 3a,b). Achieving similar death levels among target cells without PNB treatment required an 18-fold higher concentration of Doxorubicin (85 μg ml^{-1}) and a 15-fold higher concentration of Paclitaxel (1 μg ml^{-1}). Therefore, the PNB mechanism overcame the drug resistance of the employed target cells and spared other cells, thus demonstrating both high therapeutic efficacy and selectivity and, in addition, allowing a significant reduction in drug dose. It should be noted that the PNB mechanism was universally efficient at releasing two principally different drugs, Doxorubicin and Paclitaxel from two principally different nanocarriers, liposomes and micelles.

Comments to Supplementary Figure 3 c,d. We used EGFR-positive HN31 (cancer) cells to estimate the importance of such co-localization by comparing the effect of plain (non-conjugated) and C225-conjugated liposomes and micelles. Plain nanocarriers increased the cancer cell viability by several-fold both for Doxorubicin (Supplementary Fig. 3c) and for Paclitaxel (Supplementary Fig. 3d) compared with the conjugated carriers. The non-specific uptake of plain nanocarriers apparently prevented their efficient mixing with gold NPs through receptor-mediated endocytosis. The high sensitivity of the PNB release mechanism to the co-localization of nanocarriers and GNPs can be explained by the localized nature of the PNB impact. Next, we used two different molecular targets in cancer cells (instead of one, EGFR, in the previous experiments), and targeted gold GNP-C225 to EGFR and Paclitaxel to nucleosomes by conjugating them to a 2C5 antibody we previously

synthesized[1]. The effect of such dual" targeting was similar to that observed for a single target, EGFR (Supplementary Fig. 3d). Therefore, the intracellular co-localization of nanocarriers and gold NPs can also be achieved by using one or several different molecular targets and matching vectors.

Comments to Supplementary Figure 3 e,f. After pre-treating both cancer and normal cells with several combinations (Supplementary Fig. 3e,f) including Ptx-C225 at a further reduced dose of Paclitaxel of 0.05 μg ml^{-1}, GNP-C225 and single laser pulses (532 nm, 70 ps, 40 mJ cm^{-2}), we exposed the same cells to a single dose of X-rays (10 Gy). The radiation treatment was administered within 60 min after PNB generation, i.e. when the intracellular concentration of the released drug was close to the maximal. The concomitant application of GNP-C225, Ptx-C225 and X-rays further reduced the viability of cancer cells to 48±4% (Supplementary Fig. 3e, "GNP+Ptx" mode), thus confirming the well-known radio-sensitizing effect of the drug. However, in all the above cases, the gains in cancer cell destruction were rather incremental and much lower than that achieved previously with the PNB-enhanced drug release without X-rays. In contrast, when the same X-ray dose was applied within 30 minutes after PNB generation in cancer cells pre-treated with Ptx-C225 and GNP-C225 (i.e. when the local intracellular concentration of the released drug was expected to be the maximal), we observed reduction in the cancer cell viability down to 10±2 % (Supplementary Fig. 3e, "Ptx +PNB" mode), 25% of the effect of the same drug and X-rays alone (Supplementary Fig. 3e, "Ptx" mode). The PNB lifetimes were 55–60 ns in cancer cells and close to zero in normal cells (Supplementary Fig. 3f). Thus, the "PNB-drug-radiation" mode provided the maximal destruction of cancer cells. The viability of normal cells after identical treatment with GNPs, the encapsulated drug, single laser pulses and X-rays remained relatively high 71 ± 5% (Supplementary Fig. 3f), thus showing the high selectivity and low non-specific toxicity of this combination. Although this experiment did not aim to optimize the radio-sensitivity of cancer cells and to measure long-term effects, it shows that plasmonic nanobubbles and nanoclusters can selectively enhance two standard therapeutics in cancer cells to overcome their resistance to therapies and to reduce non-specific toxicity.

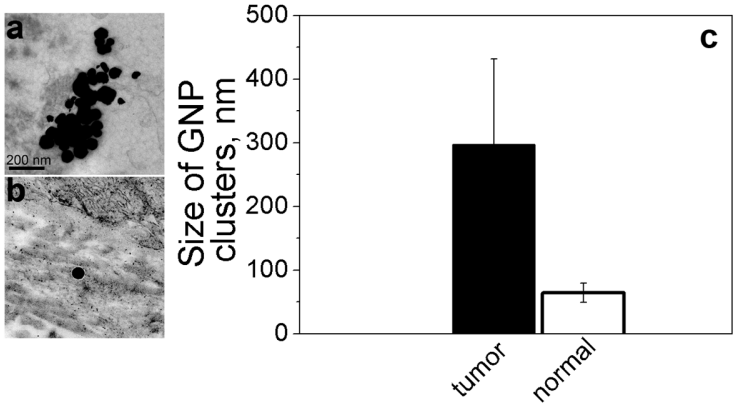

Supplementary Figure 4. Transmission electron microscopy images of solid 60 nm GNP-C225 conjugates in tumor (**a**) and adjacent muscle tissue (**b**) 24 h after systemic injection of GNP-C225 into the mouse; (**c**) average size of GNP clusters in tumor and adjacent tissue (according to TEM images).

Comments to Supplementary Figure 4. The evaluation of GNP clustering *in vivo* was done using TEM microscopy (Hitachi H-7500 Electron Microscope) (Supplementary Fig. 4a-c). Twenty-four hours after the systemic injection of GNP-C225 conjugates (0.8μg g^{-1}), the tumor and adjusted normal tissues were extracted and prepared using the standard technique for TEM imaging. The big GNP clusters were observed solely in the tumor and only small clusters or single GNPs were detected in normal tissue.

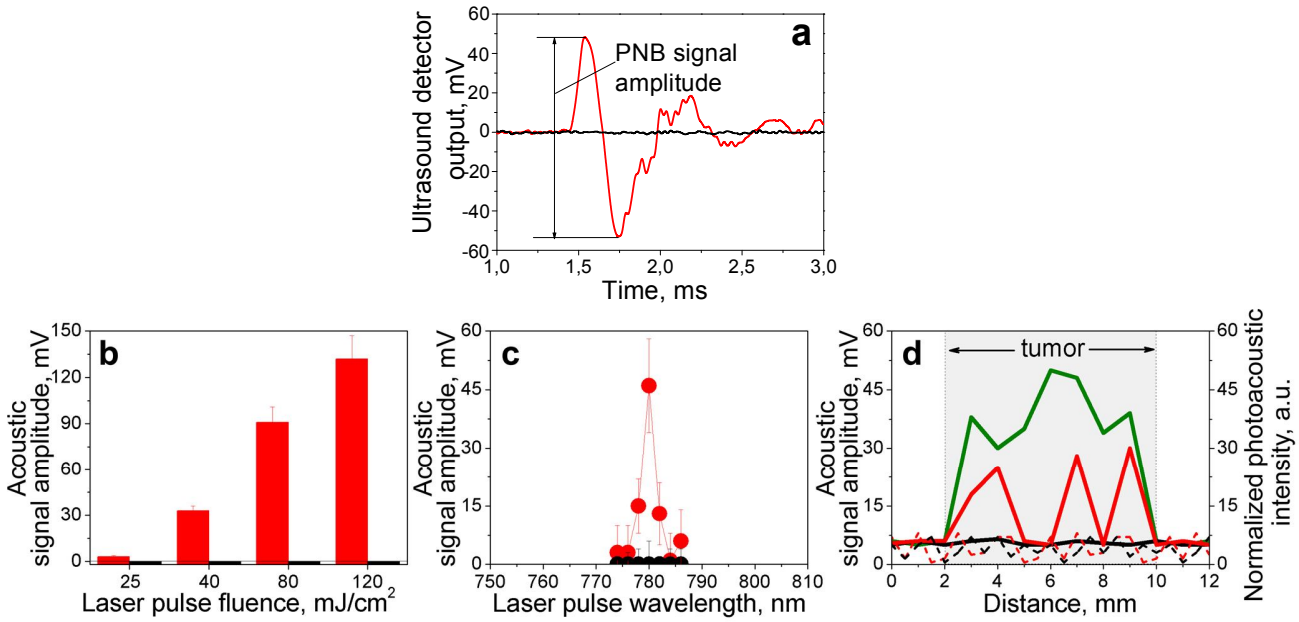

Supplementary Figure 5. Acoustic detection of PNBs *in vivo*. (**a**) Acoustic responses to a single laser pulse (780 nm, 45 mJ cm^{-2}) from a primary tumor (*red*) and adjacent normal tissue (*black*) in a mouse systemically treated with GNP-C225 conjugates. (**b**) Amplitude of the PNB acoustic response as function of the laser pulse fluence in tumor (red) and normal tissue (black) *in vivo* in a mouse systemically treated with GNP-C225 conjugates [135]. (**c**) Spectra of acoustic responses of a tumor (*red*) and intact tissue (*black*) after systemic delivery of GNP-C225 conjugates in a mouse. Acoustic responses were obtained 24 hours after the systemic GNP-C225 injection [135]. (**d**) Scans of GNP-treated animal: PNB signal amplitudes for primary tumor (*solid green*), surgical margins after tumor resection (*solid red*) and primary tumor in intact animal that was not treated with GNPs (*solid black*), standard photoacoustic small animal imaging system (Vevo LAZR, Visual Sonics) signals for the same animals with untreated (*black dashed line*) and GNP-treated primary tumors (*red dashed line*).

Comments to Supplementary Figure 5. The GNP cluster-threshold mechanism of PNB generation

provides the ultimate cancer cell specificity of PNBs (Supplementary Fig. 5) via the formation of the largest GNP clusters only in cancer cells, through receptor-mediated endocytosis of GNPs (Supplementary Fig. 4). The selectivity of PNBs generated *in vivo* was evaluated with a 70 ps laser pulse at different laser pulse fluences (Supplementary Fig. 5b) 24 hours after the systemic injection of GNP-C225 conjugates in mice. The diameter of the excitation laser beam was 470 μm in this study. The maximal diameter of the PNB was measured *in vivo* through the acoustical responses (Supplementary Fig. 5a)[2]. The PNB diameter was easily controlled via the laser pulse fluence (Supplementary Fig. 5b) with very high, 2 – 4 nm wide, spectral selectivity (Supplementary Fig. 5c).

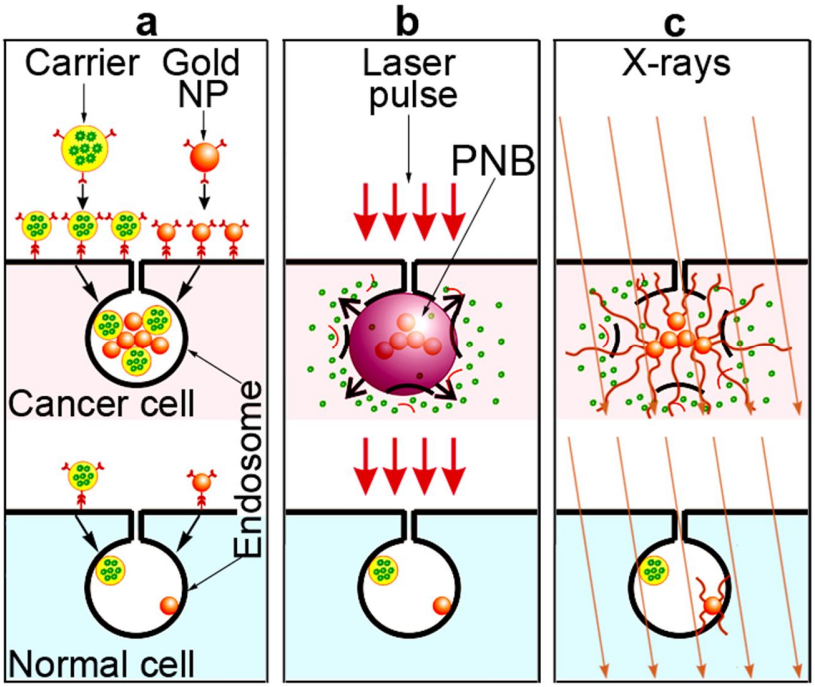

Supplementary Figure 6. Three-step quadrapeutics protocol amplifies the therapeutic efficacy and cancer specificity of chemoradiation therapy. (**a**) Systemic administration of low doses of GNPs and drug-loaded nanocarriers results in the large mixed intracellular clusters of GNPs and drug nanocarriers which are self-assembled by cancer cells (top), but not by normal cells (bottom). (**b**) Local administration of a single laser pulse results in the cancer-cell specific generation of a plasmonic nanobubble (PNB) that delivers the localized intracellular mechanical impact and ejection of the encapsulated drug (green dots) into cytoplasm. In normal cells non-specific uptake of fewer GNPs is insufficient to generate PNBs and no drug release is triggered. (**c**) Local administration of low dose of X-rays results in their intracellular amplification by a GNP cluster. Intracellular co-localization of these three therapeutic mechanisms results in their synergy which amplifies the therapeutic efficacy of low entry therapeutic in cancer cells but not in normal cells.

Supplementary Methods

Calcein Green dye-loaded liposomes. Liposomes were prepared by the lipid film hydration method. A chloroform solution of ePC and cholesterol (70:30 molar ratio) was evaporated by rotary evaporation followed by freeze-drying. The film was then hydrated in 1 ml 50mM Calcein Green solution. The resulting multilamellar liposome solution was then extruded 11 times through a 200 nm pore sized Nuclepore polycarbonate membrane (Whatman) using an Avanti hand extrusion device (Avanti Polar Lipids). After extrusion, the extraliposomal calcein buffer was removed by gel filtration on a BioGel 1.5M. The size of the Calcein-loaded liposomes was 149.23± 23 nm respectively. The conjugation of the liposomes with antibody 2C5 to cancer-specific nucleosomes[1], did not change the liposome size significantly.

The fluorescence signals of both intact Calcein Green-loaded liposomes and those dissolved with alcohol, were tested by using a LSM710 laser confocal microscope (Carl Zeiss MicroImaging GmbH, Germany). The liposome suspension was mixed with alcohol (10:1 ratio) and the thin (3 μm) samples of intact and dissolved liposomes were prepared between two pieces of glass. The high concentration of the dye in the liposomes caused significant quenching that dimmed its fluorescence in the intact liposomes. In a suspension test, the liposomes that had been dissolved with alcohol caused an increase in the level of green fluorescence by 16-fold. Three samples were prepared and imaged for intact and test groups.

Synthesis and characterization of drug nanocarriers. Paclitaxel was incorporated in $mPEG_{2000}$–PE micelles by the lipid film hydration method. Briefly, 0.1 mg of paclitaxel (10 mg ml^{-1} in methanol) was mixed with a $mPEG_{2000}$–PE solution in chloroform. The organic solvents were removed by rotary evaporation followed by freeze-drying. The film was hydrated with 10mM phosphate-buffered saline (PBS), pH 7.4 at room temperature and vortexed for 5 minutes to give a final lipid concentration of 5mM. The unincorporated drug was removed by filtration of the micelle suspension through 0.2μm

membrane filters. *Synthesis of pNP-PEG$_{3400}$-PE conjugate*. In order to prepare antibody (mAb 2C5/ mAb C225)-modified micelles and liposomes, we first conjugated the antibody to the distal tips of PEG blocks via p-nitrophenylcarbonyl (pNP) groups (using a pNP-PEG$_{3400}$-PE conjugate) to form antibody-PEG$_{3400}$-PE conjugate. Modification of drug–loaded mPEG$_{2000}$–PE micelles or Calcein-loaded liposomes or Doxil with this conjugate was done using the post-insertion method[3-5]. The pNP-PEG$_{3400}$-PE was synthesized and purified according to a previously established method[6]. Briefly, the DOPE was mixed with a 5-fold molar excess of PEG-(pNP)$_2$ in chloroform in the presence of triethylamine. Organic solvents were removed, the resultant pNP-PEG$_{3400}$-PE micelles were separated from free PEG and pNP on a sepharose CL-4B column. The product pNP-PEG$_{3400}$-PE obtained was freeze-dried and stored in chloroform at − 80 °C. *Preparation of antibody-PEG$_{3400}$-PE conjugate and preparation of targeted-micelles and liposomes.* The chloroform solution of reactive component, pNP-PEG$_{3400}$-PE (32 molar excess over antibody) was evaporated and freeze-dried to form a film in a small test tube. The dried film was hydrated with 5mM citrate buffered saline pH 5.5 containing 10mg ml^{-1} octyl glucoside followed by the addition of antibody solution in PBS pH 7.4 or water. The pH was adjusted to 8.0-8.5 with 100 mM phosphate buffer pH 8.5. The reaction was continued overnight at 4°C. The next day, the micelles were dialyzed against 1L of 10 mM PBS, pH 7.4 using cellulose ester membranes with a cut-off size of 300 kDa. The amount of antibody in the antibody-PEG$_{3400}$-PE conjugate was estimated by a bicinchoninicacid (BCA) protein assay with pure antibody as the standard. The drug loaded PEG$_{2000}$-PE micelles (0.5ml) were incubated overnight with antibody-PEG$_{3400}$-PE conjugate (equivalent to 0.487 mg of antibody) to prepare targeted micelles. To prepare 2C5 or C225-targeted liposomes, 1ml of liposomes were incubated overnight with antibody-PEG$_{3400}$-PE conjugate (equivalent to 0.150 mg of antibody). *Characterization of micelles and liposomes***.** The micelle and liposome size (hydrodynamic diameter) was measured by dynamic light scattering (DLS) using a N4 Plus Submicron Particle System (Coulter Corporation, Miami, FL, USA). The micelle and liposome suspensions were diluted with deionized, distilled water until a concentration providing a light scattering intensity of 5×10^4 to

1×10^6 counts/sec was achieved. The particle size distribution of all samples was measured in triplicate. The size of the Paclitaxel-loaded micelles was 14.5 ± 0.11 nm. Antibody modification did not change the micelle/liposome size significantly.

The amount of Paclitaxel in the micelles was measured by reversed phase-HPLC. The micelles were diluted with the mobile phase prior to application to the HPLC column. The samples were analyzed by reversed phase-HPLC. A D-7000 HPLC system equipped with a diode array and fluorescence detector (Hitachi, Japan) and Symmetry C18 column, 4.6 mm × 250 mm (Waters, Milford, MA, USA) was used. The column was eluted with water /acetonitrile (30:70 % v/v) at 1.0 ml min^{-1}. Paclitaxel was detected at 227 nm. The injection volume was 50 μL. All samples were analyzed in triplicate. The amount of Paclitaxel loaded in plain $mPEG_{2000}$-PE and antibody-modified $mPEG_{2000}$-PE micelles was found to be 0.1mg ml^{-1} and 0.08mg ml^{-1} respectively. The amount of Doxorubicin in liposomes was determined after the treatment of the liposome sample with 1% Triton-100 using plate reader (Synergy HT multimode microplate reader, BioTek Instrument, Winooski, VT) with 485/590 nm excitation/emission wavelengths[7].

EGFR expression in cells. We used multi-drug resistant and fast-growing HN31 squamous carcinoma cells (associated with head and neck cancers) which are expressed by the epidermal growth factor receptor (EGFR), and slow-growing indolent HN30 HNSCC which have a 2.0 times lower level of EGFR expression than HN31 cells and immortalized normal human oral kerotinocyte NOM9 cells which have a 2.8 times lower level of EGFR expression than HN31 cells. These cell lines were kindly provided by Drs. J. Myers and and J. Ensley.

Animal models. Healthy, male athymic nude mice, aged 8 to 12 weeks, were purchased from the National Cancer Institute-Frederick Cancer Research and Development Center (Frederick, MD) and used in accordance with Animal Care Use Guidelines under the protocols approved by IACUC of the

Texas MD Anderson Cancer Center and by IACUC of Rice University. Two different established models of HNSCC were used:

1. Recurrent disease[8-10]. This model used a reduced number of HNSCC cells: 180,000 of the *in vitro* pre-treated HN31 cells were injected on the mice flanks for the modeling of *local recurrent disease*. Four groups of cells were used: (1) intact cells, (2) cells treated *in vitro* by Doxil (2 μg ml^{-1}) and X-rays (4 Gy) and cells treated with PNBs (without drugs or X-rays), (3) cells treated with Doxil (2 μg ml^{-1}) and X-rays (4 Gy) and cells treated with quadrapeutics (Doxil: 2 μg ml^{-1}, GNP: $2.4x10^{10}$ particles ml^{-1}, laser pulse: 45 mJ cm^{-2} in 24 hours after GNP administration, X-rays: 4 Gy, 6 hours after laser treatment). All animals were monitored on a daily basis. Tumor volume was estimated as half of the small diameter squared multiplied by the large diameter[11].

2. Primary xenograft HNSCC tumors were induced s.c. by injecting 0.5 mln of Luciferase-encoded HN31 cells and was grown to 3-5 mm. Tumors were quantified weekly via their volume (measured with a caliper) and Luciferase-induced bioluminescence (measured via small animal imaging system IVIS Lumina). One group received no treatment (6 animals), other three groups received the following single primary treatments: Quadrapeutic group (11 animals) received GNP-C225s (0.8 μg g^{-1}) and Doxil-C225 (1mg kg^{-1}) via intra-venous concomitant injection. In 24 hours tumor areas (15 x 15 mm) were scanned with broad near-infrared laser pulses (780 nm, 45 mJ cm^{-2}) and then after 6 hours were exposed to X-rays (4 Gy). PNB group (4 animals) received identical doses of GNP and laser pulses. Generation of PNBs in tumors was monitored with ultrasound detector during the laser scan (Fig. 6a). Chemoradiation group (11 animals) received identical doses of drug and X-rays as the quadrapeutic group. All animals were monitored for three weeks, the period that stably showed a moribund condition among untreated animals.

Bioluminescent imaging was performed with a highly sensitive, cooled CCD camera mounted in a light-tight specimen box, using protocols similar to those described previously[12,13]. Imaging and quantification of signals were controlled by the acquisition and analysis software Living Image. For *in*

vivo imaging, animals were given the substrate D-luciferin by intraperitoneal injection at 150 mg kg^{-1} in DPBS Dulbecco's Phosphate Buffered Saline (Invitrogen, Carlsbad, CA, USA), and anesthetized (1–3% isoflurane). The mice were then placed onto the warmed stage inside the light-tight camera box with continuous exposure to 1–2% isoflurane. Imaging time was 10 s. Generally, two to three mice were imaged at a time.

3. MRD model.[14] The tumors were xenografted with the HN31 cells as previously described[15]. The tumors were induced on the mice flanks: the nude mice were anesthetized and $1x10^6$ HN31 encoded with GFP cells was injected using a 1-ml tuberculin syringe with a 30-gauge hypodermic needle. 14 to 17 days after the cell injection, when the tumors were already established (5-7 mm in diameter), the GNP-C225 (0.8μg g^{-1} of body weight) and/or Doxil-C225 (1 mg kg^{-1} of body weight) conjugates were injected into the anesthetized mice via the tail vein using an intravenous catheter and a 1-ml-insulin-syringe. Twenty-four hours after GNP and drug injection, the tumors were fully resected and the surgical margins were exposed to a scanning laser beam (70 ps, 780 nm, 45 mJ cm^{-2}, 470 μm diameter) to generate PNBs and to detect them via acoustic responses. Acoustic detection employed the generation of the pressure transients during the PNB expansion and collapse, complemented optical scattering detection, and, most importantly for the diagnostic application, provided the *in vivo* detection of PNBs in opaque tissue. The amplitude of the acoustic response was used as the PNB metric and was correlated to the optically measured lifetime of the PNB[2].

The local recurrence of HNSCC was monitored in the animals by visual observation on a daily basis. Also the small animal imaging of GFP fluorescence was performed with an IVIS Lumina Imaging System. The probability of tumor recurrence and GFP-fluorescence signals were analyzed. All animals were monitored for tumor growth on a daily basis.

Supplementary Table 1. Side-by-side comparison of current approaches with quadrapeutics.

Current Method		Limitation	Quadrapeutics Solution
Drug delivery with various nano-particles[16-57]	1.	Low release efficacy due to slow diffuse release of the drug (> 10 min)	Radically enhanced efficacy (> 3 fold) due to high speed of intracellular drug release
	2.	No on-demand release	On-demand release within nanoseconds due to explosive localized disruption of nanocarriers
	3.	High dose of the drug	90-98% reduction in the drug dose
	4.	High non-specific toxicity due to the uptake of nanoparticles by normal cells/tissues	Low non-specific toxicity due to high cancer cell selectivity of PNBs
	5.	Long treatment time	Short single laser pulse treatment
Drug delivery and therapy with: • ***External energy***[16,17,27-34,44,45,58-90] • ***GNPs***[27-34,44,45,74-79,91-93] • ***Theranostic nanoparticles***[16,17,33,34,44]	1.	Low selectivity of the drug release due to uptake of nanoparticles by normal tissues and a de-localized release mechanism	High selectivity of the drug release due to high cancer cell selectivity of PNBs
	2.	Complex and unstable nanocarriers	Simple, safe clinically-validated one-component GNPs and drug nanocarriers self-assembled by cancer cells into mixed clusters
	3.	High energy (> 1 J/cm^2)	Low energy (< 50 mJ/cm^2)
	4.	Prolonged exposure time (> 1 min)	Single laser pulse treatment (<1 second)
	5.	High non-specific toxicity	Low non-specific toxicity
Laser micro-surgery and thermal therapy[94-98]	1.	High energy due to the bulk photothermal mechanisms	Low energy due to intracellular PNB mechanism
	2.	Therapeutic selectivity depends upon laser beam pointing and size	Single cancer cell selectivity does not depend on laser beam pointing accuracy or size
	3.	May not prevent recurrence of HNSCC	Will prevent recurrence of HNSCC
GNP-mediated thermal therapy[43-45,99-126]	1.	Low selectivity within a laser aperture due to thermal diffusion	Single cancer cell selectivity does not depend upon laser beam size, no thermal impact
	2.	High dose and exposure time	Low dose and single pulse exposure
	3.	High non-specific toxicity	Low non-specific toxicity
	4.	Limited efficacy	High efficacy of explosive, non-thermal mechanism
GNP-enhanced radiotherapy[127-133]	1.	Low therapeutic gain (<2-fold)	High therapeutic gain (10-100-fold)
	2.	High GNP dose	Reduced to 0.01% GNP dose
	3.	Low selectivity of external X-rays and non-specific uptake of GNPs by normal cells and tissues	High selectivity and gain in X-ray amplification due to cancer cell-specific large GNP clusters

References

1. Sawant, R.R. & Torchilin, V.P. Polymeric micelles: polyethylene glycol-phosphatidylethanolamine (PEG-PE)-based micelles as an example. *Methods. Mol. Biol.* **624**, 131-149 (2010).
2. Lukianova-Hleb, E.Y. & Lapotko, D.O. Experimental techniques for imaging and measuring transient vapor nanobubbles. *Appl. Phys. Lett.* **101**, 264102 (2012).
3. Allen, T.M., Sapra, P. & Moase, E. Use of the post-insertion method for the formation of ligand-coupled liposomes. *Cell. Mol. Biol. Lett.* **7**, 889-894 (2002).
4. Ishida, T., Iden, D.L. & Allen, T.M. A combinatorial approach to producing sterically stabilized (Stealth) immunoliposomal drugs. *FEBS Lett.* **460**, 129-133 (1999).
5. Lukyanov, A.N., Elbayoumi, T.A., Chakilam, A.R. & Torchilin, V.P. Tumor-targeted liposomes: doxorubicin-loaded long-circulating liposomes modified with anti-cancer antibody. *J. Control. Release.* **100**, 135-144 (2004).
6. Torchilin, V.P., *et al.* p-Nitrophenylcarbonyl-PEG-PE-liposomes: fast and simple attachment of specific ligands, including monoclonal antibodies, to distal ends of PEG chains via p-nitrophenylcarbonyl groups. *Biochim. Biophys. Acta* **1511**, 397-411 (2001).
7. Wang, T., *et al.* Enhanced binding and killing of target tumor cells by drug-loaded liposomes modified with tumor-specific phage fusion coat protein. *Nanomedicine (Lond).* **5**, 563-574 (2010).
8. Ito, S., *et al.* Expression of a chemokine BRAK/CXCL14 in oral floor carcinoma cells reduces the settlement rate of the cells and suppresses their proliferation in vivo. *Biomed. Res.* **31**, 199-206 (2010).
9. Crea, F., *et al.* Pharmacologic disruption of Polycomb Repressive Complex 2 inhibits tumorigenicity and tumor progression in prostate cancer. *Mol. Cancer.* **10**, 40 (2011).
10. Lin, W.L., Liang, W.H., Lee, Y.J., Chuang, S.K., Tseng, T.H. Antitumor progression potential of caffeic acid phenethyl ester involving p75(NTR) in C6 glioma cells. *Chem. Biol. Interact.* **188**, 607-615 (2010).
11. Rofstad, E.K. & Brustad, T. Tumour growth delay following single dose irradiation of human melanoma xenografts. Correlations with tumour growth parameters, vascular structure and cellular radiosensitivity. *Br. J. Cancer.* **51**, 201-210 (1985).
12. Jenkins, D.E., *et al.* Bioluminescent imaging (BLI) to improve and refine traditional murine models of tumor growth and metastasis. *Clin. Exp. Metastasis* **20**, 733-744 (2003).

13. Rehemtulla, A., *et al.* Rapid and quantitative assessment of cancer treatment response using in vivo bioluminescence imaging. *Neoplasia* **2**, 491-495 (2000).
14. Behren, A., *et al.* Development of an oral cancer recurrence mouse model after surgical resection. *Int. J. Oncol.* **36**, 849-855 (2010).
15. Jiffar, T., *et al.* KiSS1 mediates platinum sensitivity and metastasis suppression in head and neck squamous cell carcinoma. *Oncogene*.**30**, 3163-3173 (2011).
16. Cho, K., Wang, X., Nie, S., Chen, Z.G. & Shin, D.M. Therapeutic nanoparticles for drug delivery in cancer. *Clin. Cancer Res.* **14**, 1310-1316 (2008).
17. Peer, D., *et al.* Nanocarriers as an emerging platform for cancer therapy. *Nat. Nanotechnol.* **2**, 751-760 (2007).
18. Dong, X. & Mumper, R.J. Nanomedicinal strategies to treat multidrug-resistant tumors: current progress. *Nanomedicine (Lond).* **5**, 597-615 (2010).
19. Meng, H., *et al.* Engineered design of mesoporous silica nanoparticles to deliver doxorubicin and P-glycoprotein siRNA to overcome drug resistance in a cancer cell line. *ACS Nano*. **4**, 4539-4550 (2010).
20. Liang, X.J., *et al.* Metallofullerene nanoparticles circumvent tumor resistance to cisplatin by reactivating endocytosis. *Proc. Natl. Acad. Sci. USA* **107**, 7449-7454 (2010).
21. Kim, D., Lee, E.S., Oh, K.T., Gao, Z.G. & Bae, Y.H. Doxorubicin-loaded polymeric micelle overcomes multidrug resistance of cancer by double-targeting folate receptor and early endosomal pH. *Small*. **4**, 2043-2050 (2008).
22. Torchilin, V.P. Cell penetrating peptide-modified pharmaceutical nanocarriers for intracellular drug and gene delivery. *Biopolymers*. **90**, 604-610 (2008).
23. Musacchio, T. & Torchilin, V.P. Recent developments in lipid-based pharmaceutical nanocarriers. *Front. Biosci*. **16**, 1388-1412 (2011).
24. Kuykendall, D.W. & Zimmerman, S.C. Nanoparticles - A very versatile nanocapsule. *Nat. Nanotechnol.* **2**, 201-202 (2007).
25. Wang, F., *et al.* Doxorubicin-tethered responsive gold nanoparticles facilitate intracellular drug delivery for overcoming multidrug resistance in cancer cells. *ACS Nano.* **5**, 3679-3692 (2011).
26. Kim, B., et al. Tuning payload delivery in tumour cylindroids using gold nanoparticles. *Nat. Nanotechnol*. **5**, 465-472 (2010).
27. Paasonen, L., *et al.* Gold-embedded photosensitive liposomes for drug delivery: triggering

mechanism and intracellular release. *J. Control. Release*. **147**, 136-143 (2010).

28. Pissuwan, D., Niidome, T. & Cortie, M.B. The forthcoming applications of gold nanoparticles in drug and gene delivery systems. *J. Control. Release*. **149**, 65-71 (2011).
29. Huschka, R., Neumann, O., Barhoumi, A. & Halas, N.J. Visualizing light-triggered release of molecules inside living cells. *Nano Lett*. **10**, 4117-4122 (2010).
30. Yao, C., Qu, X., Zhang, Z., Huttmann, G. & Rahmanzadeh, R. Influence of laser parameters on nanoparticle-induced membrane permeabilization. *J. Biomed. Opt.* **14**, 054034 (2009).
31. Braun, G.B., *et al.* Laser-activated gene silencing via gold nanoshell-siRNA conjugates. *ACS Nano*. **3**, 2007-2015 (2009).
32. Schomaker, M., et al. Plasmonic perforation of living cells using ultrashort laser pulses and gold nanoparticles. *SPIE Proc*. **7192**, 71920U (2009).
33. Qin, G., *et al.* Partially polymerized liposomes: stable against leakage yet capable of instantaneous release for remote controlled drug delivery. *Nanotechnology*. **22**, 155605 (2011).
34. Wu, G.H., *et al.* Remotely triggered liposome release by near-infrared light absorption via hollow gold nanoshells. *J. Am. Chem. Soc.* **130**, 8175-8177 (2008).
35. Lopez-Davila V, Seifalian AM, Loizidou M. Organic nanocarriers for cancer drug delivery. *Curr. Opin. Pharmacol*. **12**, 1-6 (2012).
36. Biswas, S., Dodwadkar, N.S., Deshpande, P.P. & Torchilin, V.P. Liposomes loaded with paclitaxel and modified with novel triphenylphosphonium-PEG-PE conjugate possess low toxicity, target mitochondria and demonstrate enhanced antitumor effects *in vitro* and *in vivo*. *J. Control. Release*. **159**, 393-402 (2012).
37. Woo, H.N., *et al.* Preclinical evaluation of injectable sirolimus formulated with polymeric nanoparticle for cancer therapy. *Int. J. Nanomedicine*. **7**, 2197-2208 (2012).
38. Sheihet, L., *et al*. Paclitaxel in tyrosine-derived nanospheres as a potential anti-cancer agent: in vivo evaluation of toxicity and efficacy in comparison with paclitaxel in Cremophor. *Eur. J. Pharm. Sci.* **45**, 320-329 (2012).
39. Sharma, A., *et al*. Activity of paclitaxel liposome formulations against human ovarian tumor xenografts. *Int. J. Cancer*. **71**, 103-107 (1997).
40. Li, X., Ding, L., Xu, Y., Wang, Y. & Ping, Q. Targeted delivery of doxorubicin using stealth liposomes modified with transferrin. *Int. J. Pharm.* 373, 116–123 (2009).
41. Rana, S., Bajaj, A., Mout, R. & Rotello, V.M. Monolayer coated gold nanoparticles for delivery applications. *Adv. Drug Deliv. Rev.* **64**, 200-216 (2012).
42. Mout, R., Moyano, D.F., Rana, S. & Rotello, V.M. Surface functionalization of nanoparticles for

nanomedicine. *Chem. Soc. Rev.* **41**, 2539-2544 (2012).

43. Dykman, L. & Khlebtsov, N. Gold nanoparticles in biomedical applications: recent advances and perspectives. *Chem. Soc. Rev.* **41**, 2256-2282 (2012).
44. Rai, P., *et al.* Development and applications of photo-triggered theranostic agents. *Adv. Drug Del. Rev.* **62**, 1094-1124 (2010).
45. Dreaden, E.C., Alkilany, A.M., Huang, X., Murphy, C.J. & El-Sayed, M.A. The golden age: gold nanoparticles for biomedicine. *Chem. Soc. Rev.* **41**, 2740–2779 (2012).
46. Northfelt, D.W., *et al.* Doxorubicin encapsulated in liposomes containing surface-bound polyethylene glycol: pharmacokinetics, tumor localization, and safety in patients with AIDS-related Kaposi's sarcoma. *J. Clin. Pharmacol.* **36**, 55-63 (1996).
47. Boulikas, T. Clinical overview on Lipoplatin: a successful liposomal formulation of cisplatin. *Expert. Opin. Investig. Drugs*. **18**, 1197-1218 (2009).
48. Hofheinz, R.D., Gnad-Vogt, S.U., Beyer, U. & Hochhaus, A. Liposomal encapsulated anti-cancer drugs. *Anticancer Drugs*. **16**, 691-707 (2005).
49. Johnstone, S., *et al.* Synergistic antitumor activity observed for a fixed ratio liposome formulation of Cytarabine (Cyt):Daunorubicin (Daun) against preclinical leukemia models. *Proc. Amer. Assoc. Cancer Res*. **46**:abstract 1405 (2005).
50. Abraham, S.A., *et al.* In vitro and in vivo characterization of doxorubicin and vincristine coencapsulated within liposomes through use of transition metal ion complexation and pH gradient loading. *Clin. Cancer Res*. **10**, 728-738 (2004).
51. Martin, F. & Boulikas, T. The challenge of liposomes in gene therapy. *Gene Ther. Mol. Biol.* **1**, 173-214 (1998).
52. Koning, G.A., Eggermont, A.M., Lindner, L.H. & ten Hagen, T.L. Hyperthermia and thermosensitive liposomes for improved delivery of chemotherapeutic drugs to solid tumors. *Pharm. Res.* **27**, 1750-1754 (2010).
53. Park, J.W., Benz, C.C. & Martin, F.J. Future directions of liposome- and immunoliposome-based cancer therapeutics. *Semin. Oncol.* **31**, 196-205 (2004).
54. Duncan, B., Kim, C. & Rotello, V.M. Gold nanoparticle platform as drug and biomacromolecule delivery systems. *J. Control. Release*. 148, 122-127 (2010).
55. Podsiadlo, P., *et al.* Gold nanoparticles enhance the anti-leukemia action of a 6-mercaptopurine chemotherapeutic agent. *Langmuir.* **24**, 568–574 (2008).
56. Andresen, T.L., Thompson, D.H. & Kaasgaard, T. Enzyme-triggered nanomedicine: Drug release strategies in cancer therapy. *Mol. Membr. Biol.* **27**, 353-363 (2010).

57. Zhu, C.-L., Lu, C.-H., Song, X.-Y., Yang, H.-H. & Wang, X.-R. Bioresponsive controlled release using mesoporous silica nanoparticles capped with aptamer-based molecular gate. *J. Am. Chem. Soc*. **133**, 1278–1281 (2011).

58. Rapoport, N.Y., Kennedy, A.M., Shea, J.E., Scaife, C.L. & Nam, K.H. Controlled and targeted tumor chemotherapy by ultrasound-activated nanoemulsions/microbubbles. *J. Control. Release*. **138**, 268-276 (2009).

59. Ferrara, K.W. Driving delivery vehicles with ultrasound. *Adv. Drug. Deliv. Rev.* **60**, 1097-1102 (2008).

60. Wang, C.H., Huang, Y.F. & Yeh, C.K. Aptamer-conjugated nanobubbles for targeted ultrasound molecular imaging. *Langmuir*. **27**, 6971-6976 (2011).

61. Xu, J.S., *et al.* Synthesizing and binding dual-mode poly (lactic-co-glycolic acid) (PLGA) nanobubbles for cancer targeting and imaging. *Biomaterials*. **31**, 1716-1722 (2010).

62. Fechheimer, M., *et al.* Transfection of mammalian cells with plasmid DNA by scrape loading and sonication loading. *Proc. Natl. Acad. Sci. USA* **84**, 8463-8467 (1987).

63. Neumann, E., Schaeferridder, M., Wang, Y. & Hofschneider, P.H. Gene-transfer into mouse lyoma cells by electroporation in high electric-fields. *EMBO. J.* **1**, 841-845 (1982).

64. Lee, S., McAuliffe, D.J., Flotte, T.J., Kollias, N. & Doukas, A.G. Photomechanical transcutaneous delivery of macromolecules. *J. Invest. Dermatol.* **111**, 925-929 (1998).

65. Qiu, Y., *et al.* The correlation between acoustic cavitation and sonoporation involved in ultrasound-mediated DNA transfection with polyethylenimine (PEI) in vitro. *J. Control. Release* **145**, 40-48 (2010).

66. Stevenson, D., *et al.* Femtosecond optical transfection of cells: viability and efficiency. *Optics Express.* **14**, 7125-7133 (2006).

67. Prentice, P., Cuschierp, A., Dholakia, K., Prausnitz, M. & Campbell, P. Membrane disruption by optically controlled microbubble cavitation. *Nat. Phys*. **1**, 107-110 (2005).

68. Kim, J.H. & Lee, T.R. Discrete thermally responsive hydrogel-coated gold nanoparticles for use as drug-delivery vehicles. *Drug Dev. Res*. **67**, 61-69 (2006).

69. Zhao, X.-Q., *et al.* Multifunctional Au@IPN-pNIPAAm nanogels for cancer cell imaging and combined chemo-photothermal treatment. *J. Mater. Chem.* **21**, 7240-7247 (2011).

70. Niidome, T., Shiotani, A., Mori, T. & Katayama, Y. Targeted delivery of gold nanorods modified with thermo-sensitive polymer. *J. Control. Release*. **148**, e65-e66 (2010).

71. Deng, Y., Yang, W., Wang, C. & Fu, S. A novel approach for preparation of thermoresponsive polymer magnetic microspheres with core–shell structure. *Adv. Mater*. **15**, 1729-1732 (2003).

72. Hribar, K.C., Lee, M.H., Lee, D. & Burdick, J.A. Enhanced release of small molecules from near-infrared light responsive polymer−nanorod composites. *ACS Nano.* **5**, 2948-2956 (2011).
73. Skirtach, A.G., *et al.* Laser-induced release of encapsulated materials inside lining cells. *Angew. Chem. Int. Ed*. **45**, 4612-4617 (2006).
74. Troutman, T.S., Leung, S.J. & Romanowski, M. Light-induced content release from plasmon-resonant liposomes. *Adv. Mater*. **21**, 2334-2338 (2009).
75. Kyrsting, A., Bendix, P.M., Stamou, D.G. & Oddershede, L.B. Heat profiling of three-dimensionally optically trapped gold nanoparticles using vesicle cargo release. *Nano Lett.* **11**, 888-892 (2011).
76. Agarwal, A., MacKey, M.A., El-Sayed, M.A. & Bellamkonda, R.V. Remote triggered release of doxorubicin in tumors by synergistic application of thermosensitive liposomes and gold nanorods. *ACS Nano*. **5**, 4919-4926 (2011).
77. Takahashi, H., Niidome, Y. & Yamada, S. Controlled release of plasmid DNA from gold nanorods induced by pulsed near-infrared light. *Chem. Commun*. **17**, 2247-2249 (2005).
78. Chen, C.C., *et al.* DNA-gold nanorod conjugates for remote control of localized gene expression by near infrared irradiation. *J. Am. Chem. Soc.* **128**, 3709-3715 (2006).
79. Jones, M.R., *et al.* Plasmonically controlled nucleic acid dehybridization with gold nanoprisms. *Chem. Phys. Chem.* **10**, 1461-1465 (2009).
80. Ibrahimkutty, S., *et al*. Ultrafast structural dynamics of the photocleavage of protein hybrid nanoparticles. *ACS Nano*. **5**, 3788-3794 (2011).
81. Lee, S.E., Liu, G.L., Kim, F. & Lee, L.P. Remote optical switch for localized and selective control of gene interference. *Nano Lett.* **9**, 562-570 (2009).
82. Lee, S.M., Park, H. & Yoo, K.H. Synergistic cancer therapeutic effects of locally delivered drug and heat using multifunctional nanoparticles. *Adv. Mater*. **22**, 4049-4053 (2010).
83. Park, J.H., *et al.* Cooperative nanoparticles for tumor detection and photothermally triggered drug delivery. *Adv. Mater.* **22**, 880-885 (2010).
84. McDannold, N.J., Vykhodtseva, N.I. & Hynynen, K. Microbubble contrast agent with focused ultrasound to create brain lesions at low power levels: MR imaging and histologic study in rabbits. *Radiology*. **241**, 95-106 (2006).
85. Coussios, C.C., Farny, C.H., Haar, G.T. & Roy, R.A. Role of acoustic cavitation in the delivery and monitoring of cancer treatment by high-intensity focused ultrasound (HIFU). *Int. J. Hyperthermia*. **23**, 105-120 (2007).
86. Liu, H.L., *et al.* Cavitation-enhanced ultrasound thermal therapy by combined low- and high-

frequency ultrasound exposure. *Ultrasound. Med. Biol*. **32**, 759-767 (2006).

87. Guzman, H.R., Nguyen, D.X., Khan, S. & Prausnitz, M.R. Ultrasound-mediated disruption of cell membranes. I. Quantification of molecular uptake and cell viability. *J. Acoust. Soc. Am*. **110**, 588-596 (2001).
88. Dijkink, R., *et al.* Controlled cavitation-cell interaction: trans-membrane transport and viability studies. *Phys. Med. Biol.* **53**, 375-390 (2008).
89. Arita, Y., *et al.* Spatially optimized gene transfection by laser-induced breakdown of optically trapped nanoparticles. *Appl. Phys. Lett.* **98**, 093702 (2011).
90. Sajja, H.K., *et al.* Development of multifunctional nanoparticles for targeted drug delivery and non-invasive imaging of therapeutic effect. *Curr. Drug. Discov. Technol.* **6**, 43-51 (2009).
91. Jang, B., Park, J.Y., Tung, C.H., Kim, I.H. & Choi, Y. Gold nanorod-photosensitizer complex for near-infrared fluorescence imaging and photodynamic/photothermal therapy in vivo. *ACS Nano*. **5**, 1086-1094 (2011).
92. Záruba, K., *et al.* Modified porphyrin-brucine conjugated to gold nanoparticles and their application in photodynamic therapy. *Org. Biomol. Chem.* **8**, 3202-3206 (2010).
93. Cheng, Y., *et al.* Highly efficient drug delivery with gold nanoparticle vectors for in vivo photodynamic therapy of cancer. *J. Am. Chem. Soc.* **130**, 10643-10647 (2008).
94. Epstein, F.J. & Farmer, J.P. Trends in surgery: laser surgery, use of the cavitron, and debulking surgery. *Neurol. Clin.* **9**, 307-315 (1991).
95. Carpentier, A., *et al.* Real-time magnetic resonance-guided laser thermal therapy for focal metastatic brain tumors. *Neurosurgery* **63** (Suppl 1):ONS21-8;discussion ONS28-9 (2008).
96. Ambrosch, P. The role of laser microsurgery in the treatment of laryngeal cancer. *Curr. Opin. Otolaryngol. Head Neck Surg*. **15**, 82-88 (2007).
97. Karni, R.J., Rich, J.T., Sinha, P. & Haughey, B.H. Transoral laser microsurgery: a new approach for unknown primaries of the head and neck. *Laryngoscope*. **121**, 1194-1201 (2011).
98. Roedel, R.M., *et al.* Transoral laser microsurgery for recurrence after primary radiotherapy of early glottic cancer. *Auris Nasus Larynx*. **37**, 474-481 (2010).
99. Nanospectra Biosciences, Inc. ClinicalTrials.gov [website on the Internet] Bethseda, MD: US National Library of Medicine; 2009. [Accessed December 13, 2011]. Pilot study of aurolase(tm) therapy in refractory and/or recurrent tumors of the head and neck. Available from: http://clinicaltrials.gov/ct2/show/NCT00848042. NLM identifier: NCT00848042.
100. El-Sayed, I.H., Huang, X. & El-Sayed, M.A. Surface plasmon resonance scattering and absorption of anti-EGFR antibody conjugated gold nanoparticles in cancer diagnostics:

applications in oral cancer. *Nano Lett.* **5**, 829-834 (2006).

101. Sokolov, K., *et al.* Real-time vital optical imaging of precancer using anti-epidermal growth factor receptor antibodies conjugated to gold nanoparticles. *Cancer Res.* **63**, 1999-2004 (2003).
102. Hildebrandt, B., *et al*. The cellular and molecular basis of hyperthermia. *Crit. Rev. Oncol. Hematol.* **43**, 33-56 (2002).
103. Kasili, P.M. & Vo-Dinh, T. Liposome encapsulated gold nanoshells for nanophototherapy induced hyperthermia. *Int. J. Nanotechnol.* **2**, 397–410 (2005).
104. Chan, W.C.W., Hauck, T.S., Jennings, T.L., Yatsenko, T. & Kumaradas, J.C. Enhancing the toxicity of cancer chemotherapeutics with gold nanorod hyperthermia. *Advan. Materials*. **20**, 3832-3838 (2008).
105. Choi, W.I., *et al*. Tumor regression in vivo by photothermal therapy based on gold-nanorod-loaded, functional nanocarriers. *ACS Nano*. **5**, 1995-2003 (2011).
106. Khlebtsov, B.N., et al.. Plasmonic nanopowders for photothermal therapy of tumors. *Langmuir*. **28**, 8994-9002 (2012).
107. Li, Z., *et al.* RGD-conjugated dendrimer-modified gold nanorods for in vivo tumor targeting and photothermal therapy. *Mol. Pharm.* **7**, 94-104 (2010).
108. Chen. J., *et al.* Gold nanocages as photothermal transducers for cancer treatment. *Small*. **6**, 811–817 (2010).
109. Curley, S.A., Cherukuri, P. & Glazer, E.S. Targeted hyperthermia using metal nanoparticles. *Adv. Drug. Deliver. Rev.* **62**, 339-345 (2010).
110. Curley, S.A., *et al.* Noninvasive radiofrequency field-induced hyperthermic cytotoxicity in human cancer cells using cetuximab-targeted gold nanoparticles. *J. Exp. Ther. Oncol.* **7**, 313-326 (2008).
111. Jain, P.K., Huang, X., El-Sayed, I.H. & El-Sayed, M.A. Noble metals on the nanoscale: optical and photothermal properties and some applications in imaging, sensing, biology, and medicine. *Acc. Chem. Res.* **41**, 1578-1586 (2008).
112. Gobin, A.M., *et al.* Near-infrared resonant nanoshells for combined optical imaging and photothermal cancer therapy. *Nano Lett.* **7**, 1929-1934 (2007).
113. Huff, T.B., *et al.* Hyperthermic effects of gold nanorods on tumor cells. *Nanomedicine (Lond).* **2**, 125-132 (2007).
114. O'Neal, D.P., Hirsch, L.R., Halas, N.J., Payne, J.D. & West, J.L. Photo-thermal tumor ablation in mice using near infrared-absorbing nanoparticles. *Cancer Lett.* **209**, 171-176 (2004).
115. Chen, W., *et al.* A molecularly targeted theranostic probe for ovarian cancer. *Mol. Cancer. Ther.*

9, 1028-1038 (2010).

116. Bernardi, R.J., Lowery, A.R., Thompson, P.A., Blaney, S.M. & West, J.L. Immunonanoshells for targeted photothermal ablation in medulloblastoma and glioma: an in vitro evaluation using human cell lines. *J. Neurooncol.* **86**, 165-172 (2008).
117. Li, J.L., *et al.* In vitro cancer cell imaging and therapy using transferrin-conjugated gold nanoparticles. *Cancer Lett*. **274**, 319-326 (2009).
118. Bardhan, R., Lal, S., Joshi, A. & Halas, N.J. Theranostic nanoshells: from probe design to imaging and treatment of cancer. *Acc. Chem. Res.* **44**, 936-946 (2011).
119. Ke, H., *et al.* Gold-nanoshelled microcapsules: a theranostic agent for ultrasound contrast imaging and photothermal therapy. *Angew. Chem. Int. Ed*. **50**, 3017-3021 (2011).
120. Cai, W., Gao, T., Hong, H. & Sun, J. Applications of gold nanoparticles in cancer nanotechnology. *Nanotechnology, Science and Applications* **1**, 17-32 (2008).
121. West, J.L., *et al.* A new era for cancer treatment: gold-nanoparticle-mediated thermal therapies. *Small*. **7**, 169-183 (2011).
122. Boisselier, E. & Astruc, D. Gold nanoparticles in nanomedicine: preparations, imaging, diagnostics, therapies and toxicity. *Chem. Soc. Rev.* **38**, 1759-1782 (2009).
123. Huang, X., Jain, P.K., El-Sayed, I.H. & El-Sayed, M.A. Gold nanoparticles and nanorods in medicine: From cancer diagnostics to photothermal therapy. *Nanomedicine*. **2**, 681-693 (2007).
124. Loo, C., Lowery, A., Halas, N., West, J. & Drezek, R. Immunotargeted nanoshells for integrated cancer imaging and therapy. *Nano Lett*. **5**, 709-711 (2005).
125. West, J.L. & Halas, N.J. Engineered nanomaterials for biophotonics applications: improving sensing, imaging, and therapeutics. *Ann. Rev. Biomed. Eng.* **5**, 285-292 (2003).
126. Pitsillides, C.M., Joe, E.K., Wei, X., Anderson, R.R. & Lin, C.P. Selective cell targeting with light-absorbing microparticles and nanoparticles. *Biophys. J.* **84**, 4023-4032 (2003).
127. Hainfeld, J.F., Slatkin, D.N. & Smilowitz, H.M. The use of gold nanoparticles to enhance radiotherapy in mice. *Phys. Med. Biol.* **49**, N309-315 (2004).
128. Leung, M.K., *et al.* Irradiation of gold nanoparticles by x-rays: Monte Carlo simulation of dose enhancements and the spatial properties of the secondary electrons production. *Med. Phys.* **38**, 624-631 (2011).
129. Zhang, X.D., *et al.* Size-dependent radiosensitization of PEG-coated gold nanoparticles for cancer radiation therapy. *Biomaterials*. **33**, 6408-6419 (2012).
130. Hainfeld, J.F., *et al.* Gold nanoparticles enhance the radiation therapy of a murine squamous cell carcinoma. *Phys. Med. Biol.* **55**, 3045-3059 (2010).

131. Jiao, P., *et al.* Leading neuroblastoma cells to die by multiple premeditated attacks from a multifunctionalized nanoconstruct. *J. Am. Chem. Soc.* **133**, 13918-13921 (2011).
132. Rahman, W.N., *et al.* Enhancement of radiation effects by gold nanoparticles for superficial radiation therapy. *Nanomedicine.* **5**, 136-142 (2009).
133. Kong, T., *et al.* Enhancement of radiation cytotoxicity in breast-cancer cells by localized attachment of gold nanoparticles. *Small*. **4**, 1537-1543 (2008).
134. Lukianova-Hleb, E.Y. *et al.* Improved cellular specificity of plasmonic nanobubbles versus nanoparticles in heterogeneous cell systems. *PLoS ONE* **7**, e34537 (2012).
135. Lukianova-Hleb, E.Y., Volkov, A.N., Wu, X. & Lapotko, D.O. Transient enhancement and spectral narrowing of the photothermal effect of plasmonic nanoparticles under pulsed excitation. *Adv. Mater*. **25**, 772–776 (2013).